VALERI PROJECT
Website: http://www.avignon.inra.fr/valeri
CAMPAIGN 2002

GROUND DATA PROCESSING & PRODUCTION OF THE LEVEL 1 HIGH RESOLUTION MAPS

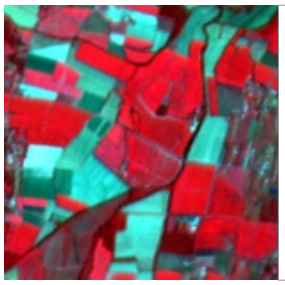

VALERI 2002

SUD-OUEST site
(crops and grassland)

Philippe Rossello, Marie Weiss, Frédéric Baret

August 2005

PLAN

1. Introduction

This report describes the production of the high resolution, level 1, biophysical variable maps for the Sud-Ouest site (Table 1 gives the coordinates) in 2002 (see campaign report for more details about the site and the ground measurement campaign: http://www.avignon.inra.fr/valeri). Level 1 map corresponds to the map derived from the determination of a transfer function between reflectance values of the SPOT image acquired during (or around) the ground campaign, and biophysical variable measurements (hemispherical images). For each Elementary Sampling Unit (ESU), the hemispherical images were processed using the CAN-EYE software (Version 3.6) developed at INRA-CSE. The derived biophysical variable maps are:

• four Leaf Area Index (LAI) are considered: effective LAI (LAIeff) and true LAI (LAItrue) derived from the description of the gap fraction as a function of the view zenith angle; effective LAI57 (LAI57eff) and true LAI57 (LAI57true) derived from the gap fraction at 57.5°, which is independent on the leaf inclination. Effective LAI and effective LAI57 do not take into account clumping effect. LAItrue and LAI57true are derived using the method proposed by Lang and Yueqin[1] (1986);

• cover fraction (fCover): it is the percentage of soil covered by vegetation. To improve the spatial sampling, fCover was computed over 0 to 10° zenith angle;

• fAPAR: it is the fraction of Absorbed Photosynthetically Active Radiation (PAR=400-700nm). The fAPAR is defined either instantaneously (for a given solar position) or integrated all over the day. Following a study based on radiative transfer model simulations, it has been shown that the root mean square error between instantaneous fAPAR computed every 30 minutes and the daily fAPAR is the lowest for instantaneous fAPAR at 10h00 AM (solar time, RMSE = 0.021). Therefore, the derivation of fAPAR from CAN-EYE corresponds to the instantaneous black sky fAPAR at 10h00 AM.

The land cover is mainly composed of crops (corn, soya, sunflowers) and grassland. The size of the fields is important since the mean size is about 20 ha. The site is quite flat. It is at about 170 m altitude (for more information, see campaign report: http://www.avignon.inra.fr/valeri).

The site coordinates are described in Table 1:

	UTM, 31 North, WGS84 (units = meters)		Geographic Lat/Lon WGS84 (units = degrees)	
	Northing	Easthing	Lat.	Lon.
Upper left corner	4820075	356002	43.51975	1.218277
Lower right corner	4817035	359042	43.492944	1.256638
Center	4818555	357522	43.506333	1.237444

Table 1. Description of the site coordinates.

The ground measurements were carried out from 07/07/2002 to 08/07/2002, while the high spatial resolution image (SPOT2, HRV1, resolution: 20 m) was acquired on 20/07/2002. The characteristics of the SPOT image are specified in the campaign report. Several images are available but the level of precision differs (radiometry, geometry…). For more information, please come into contact with Philippe Rossello.

2. Available data

2.1. SPOT Image

The SPOT image was acquired the 20th July 2002 by HRV1 on SPOT2. It was geo-located by SPOTimage (SPOTView basic). The projection is UTM 31 North, WGS84 (please, refer to the campaign report for more details: http://www.avignon.inra.fr/valeri) and no atmospheric correction was applied to the image[2]. However, as the SPOT image is used to compute empirical relationships between reflectance and biophysical variable, we can assume that the effect of the atmosphere is the same over the whole 3.08 x 3.08 km site. Therefore, it will be taken into account everywhere in the same way.

[1] Lang, A.R.G. and Yueqin, X., 1986. Estimation of leaf area index from transmission of direct sunlight in discontinuous canopies. Agric. For. Meteorol., 37: 229-243.
[2] Atmospheric data were available, but the radiometry of the image corrected by the CESBIO was bad.

Figure 1 shows the relationship between RED and near infrared (NIR) SPOT channels: the soil line is well marked and no saturated points are observed.

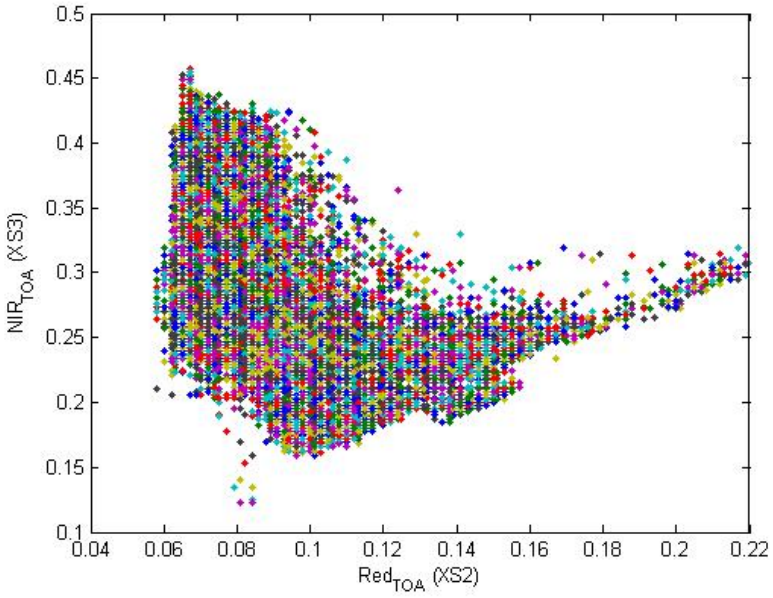

Figure 1. Red/NIR relationship on the SPOT image for Sud-Ouest, 2002.

2.2. Hemispherical images

The hemispherical images were processed by the CAN-EYE software (Version 3.6) to derive the biophysical variables. Figure 2 and Figure 3 show the distribution of the several variables over the sampled ESUs. As there was understorey in most of the ESUs, hemispherical images were acquired from above the understorey and from below the canopy (trees). The two sets of acquisition were processed separately to derived LAI (effective and true), LAI57 (effective and true), fCover, and fAPAR. The ESU biophysical variable was then computed as:

- LAIeff, LAI57eff, LAItrue, LAI57true: LAI(above) + LAI(below).
- fCover: 1-(1-fCover(above))*(1-fCover(below)). This assumes that independency of the gaps inside the understorey and the gaps inside the trees which is not true at all the scales but it is the only way to get the total fCover. However, for the local scales considered, this might be true as a first order approximation.
- fAPAR: [1-(1-fAPAR(below))*(1-fAPAR(above))], since 1-fAPAR can be considered equivalent to a gap fraction. Here again, the same independency between the two layers has to be assumed.

Note that LAI (effective and true) derived from directional gap fraction and LAI derived from gap fraction at 57.5° (effective and true) are consistent (Figure 3). Effective LAI (LAIeff, LAI57eff) varies from 0 to 8, while true LAI (LAItrue, LAI57true) varies from 0 to 10. This range shows a quite heterogeneous site in terms of LAI. The ESUs have actually effective LAI (LAIeff, LAI57eff)>2 and true LAI (LAItrue, LAI57true)>3 since the value 0 corresponds to S1, S2, S3, S4 and S5. For values, LAIeff and LAI57eff are lower than LAItrue and LAI57true. This is due to the clumping observed for several ESUs. The relationship between fAPAR and LAI is in agreement with what is expected (beer lambert law) while the fCover-LAI relationship is more noisy.

To build the relationships between biophysical variables and SPOT data, the reflectance of a given forest ESU was considered as the average reflectance over the central pixel + the 8 surrounding pixels, whereas, for crops, we took the reflectance of the pixel corresponding to the ESU. This takes into account the fact that the height of the trees are about 15 m and consequently the fish-eye observes an area of $\pi \, x \, [15 \, x \, \tan(60°)]^2 \cong 2200$ m², *i.e.* rather close to the area of 9 SPOT pixels (=3600m²) when using a maximum view zenith angle of 60°.

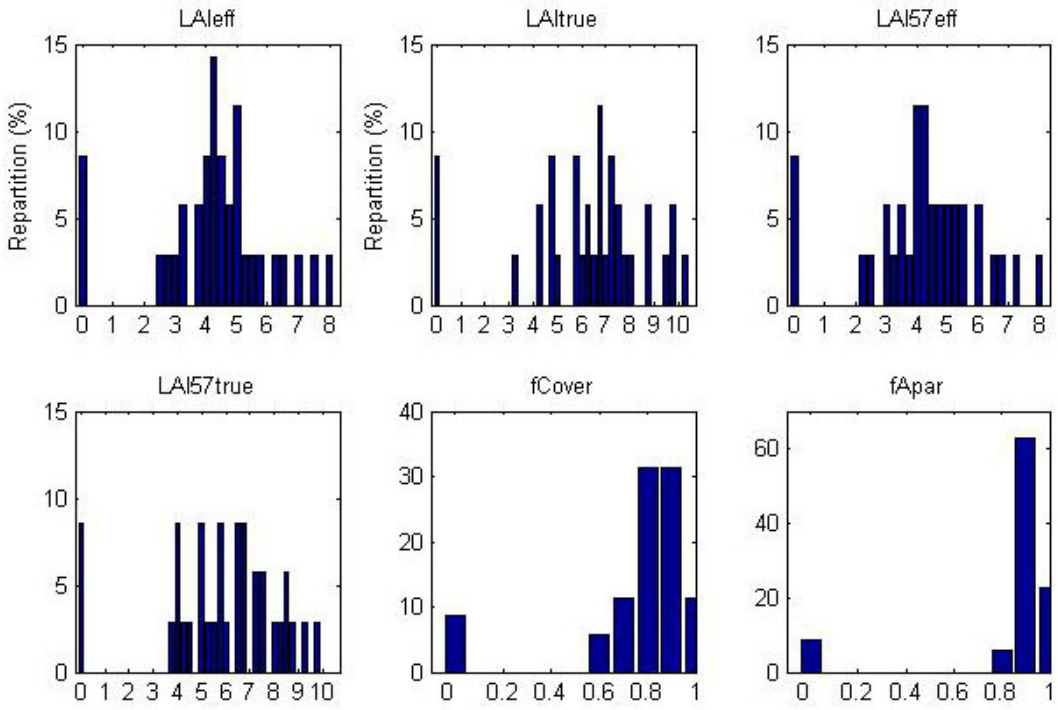

Figure 2. Distribution of the measured biophysical variables over the ESUs.

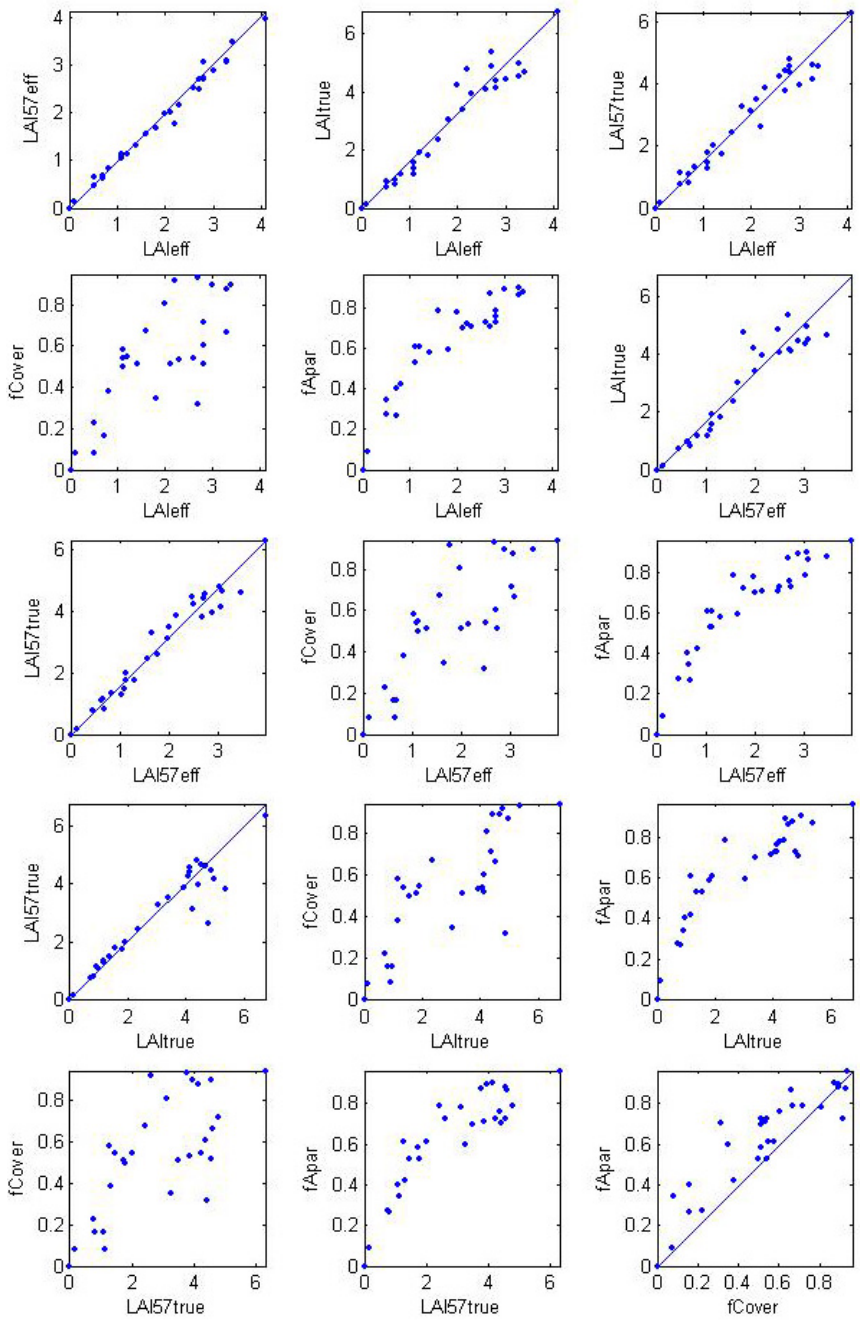

Figure 3. Relationships between the different biophysical variables

Figure 4 shows the relationships observed between the biophysical variables and the corresponding NDVI on the ESUs, as a function of the SPOT classes determined in §2.3.3. The additional ESUs (S1, S2, S3, S4 and S5) improve the relationships between the biophysical variables and corresponding NDVI. Even if no different behaviour between the classes can be observed, one ESU (CB9) in class 3 (blue) differs from the others: it is located in a fallow crop covered with "green" weed.

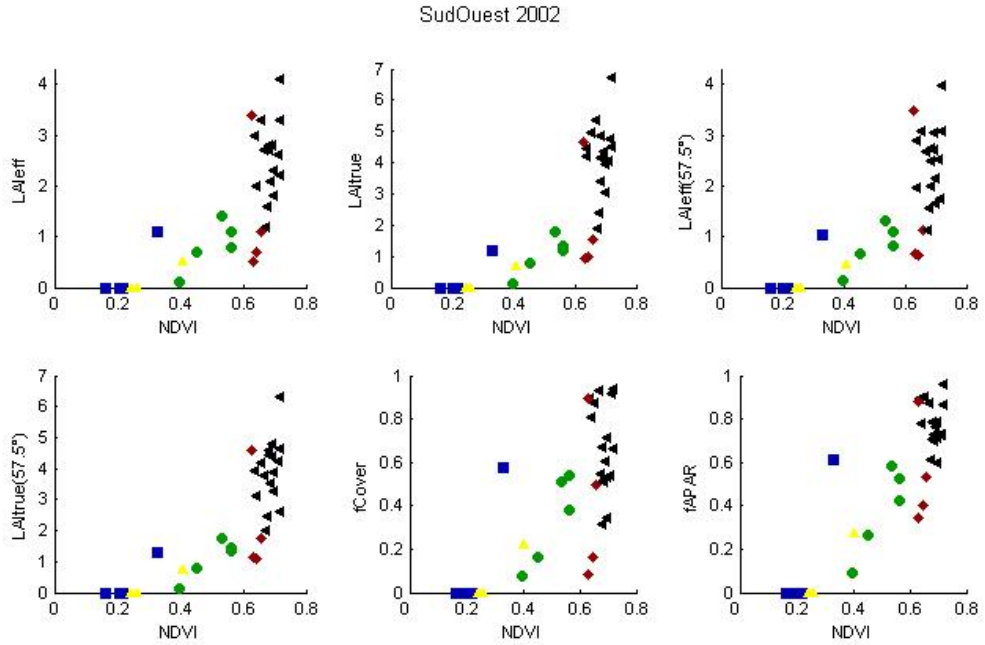

Figure 4. NDVI-Biophysical Variable relationships as a function of SPOT classes

2.3. Sampling strategy

2.3.1. Principles

The sampling strategy is defined in the campaign report: http://www.avignon.inra.fr/valeri. Each ESU was sampled based on twelve elementary photographs organized in a cross pattern.

Figure 5 shows that the 30 ESUs[3] are evenly distributed over the site (3.08 x 3.08 km). The processing of the ground data has shown that:

- ESUs CA09 and CB13 (in black on Figure 5) were located on a small plot with a strong heterogeneity on the borders. These two ESUs were eliminated;
- considering that SPOT geo-location and GPS measurements are associated to errors, we found that processed LAI for ESUs CA04, CB05, CB12 and CB14 did not correspond to the SPOT pixel in terms of reflectance as compared to the knowledge of the land use: they have been shifted by 1 or 2 pixels.

To improve the establishment of the transfer function, 5 ESUs (S1, S2, S3, S4 and S5) located over fully senesced or harvested wheat fields were considered additionally. A LAI value of 0.0 was assigned to these ESUs.

Finally 33 ESUs have been kept for the computation of the transfer function (Figure 5).

[3] 11 corn, 6 soya, 5 sunflowers, 3 grassland, 3 fallow, 1 woodland, 1 poplars.

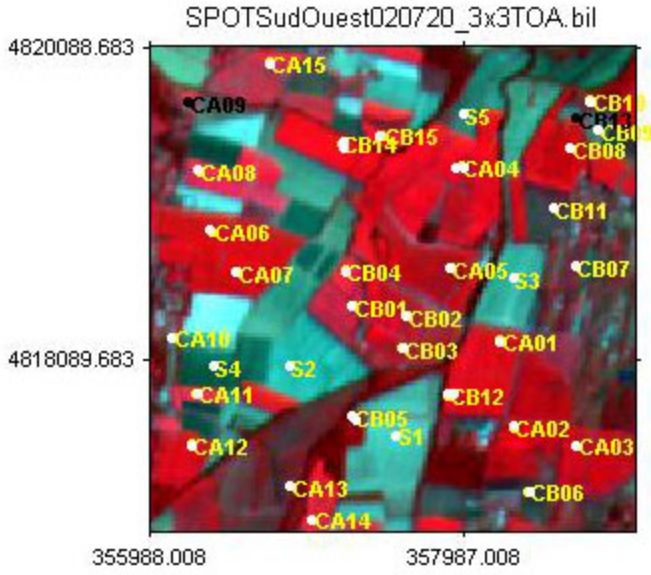

Figure 5. Distribution of the ESUs around the Sud-Ouest site. ESUs in black (CA09 and CB13) were eliminated for the computation of the transfer function.

Figure 6 shows the land cover of the Sud-Ouest site characterized by a mosaic of crops and grassland. The land cover map included here is approximative.

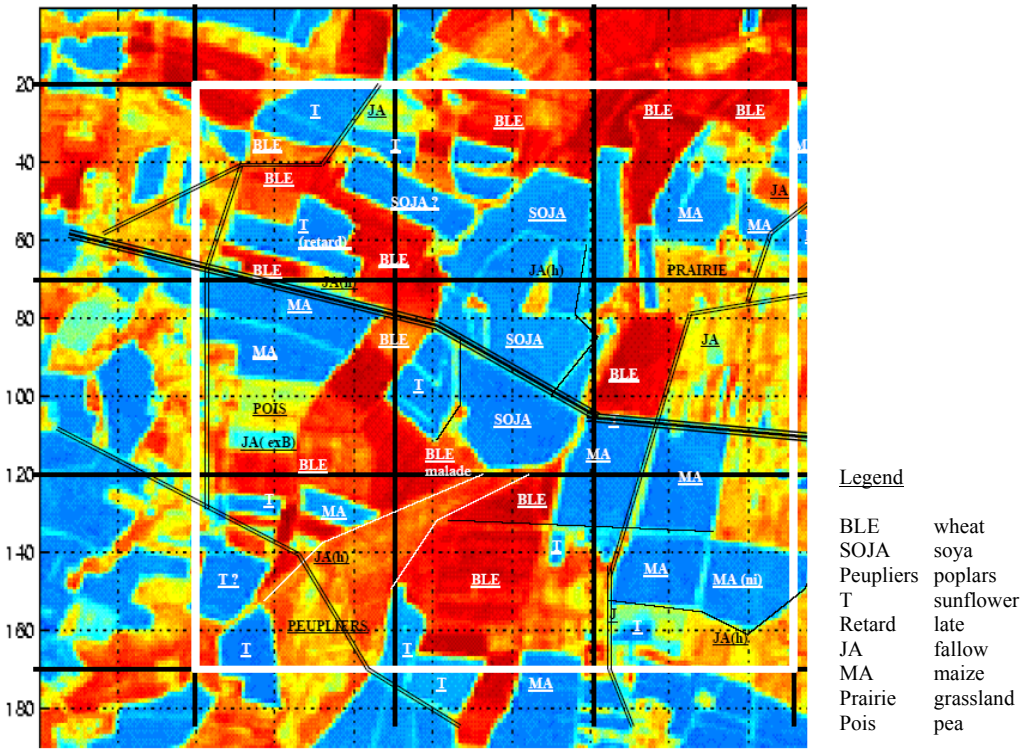

Figure 6. Land cover map[4] of the Sud-Ouest site (CESBIO, 2002).

2.3.2. Evaluation based on NDVI values

The sampling strategy is evaluated using the SPOT image by comparing the NDVI distribution over the site with the NDVI distribution over the ESUs (Figure 7). As the number of pixels is drastically different for the ESU

[4] Background map: NDVI derived from a SPOT image acquired before the campaign (document given for information, CESBIO, 2002).

and whole site (WS=22500 in case of a 3x3 km SPOT image), it is not statistically consistent to directly compare the two NDVI histograms. Therefore, the proposed technique consists in comparing the NDVI cumulative frequency of the two distributions by a Monte-Carlo procedure which aims at comparing the actual frequency to randomly shifted sampling patterns. It consists in:

1. computing the cumulative frequency of the N pixel NDVI that correspond to the exact ESU locations;
2. then, applying a unique random translation to the sampling design (modulo the size of the image);
3. computing the cumulative frequency of NDVI on the randomly shifted sampling design;
4. repeating steps 2 and 3, 199 times with 199 different random translation vectors.

This provides a total population of $N = 199 + 1$(actual) cumulative frequency on which a statistical test at acceptance probability $1 - \alpha = 95\%$ is applied: for a given NDVI level, if the actual ESU density function is between two limits defined by the $N\alpha/2 = 5$ highest and lowest values of the 200 cumulative frequencies, the hypothesis assuming that WS and ESU NDVI distributions are equivalent is accepted, otherwise it is rejected.

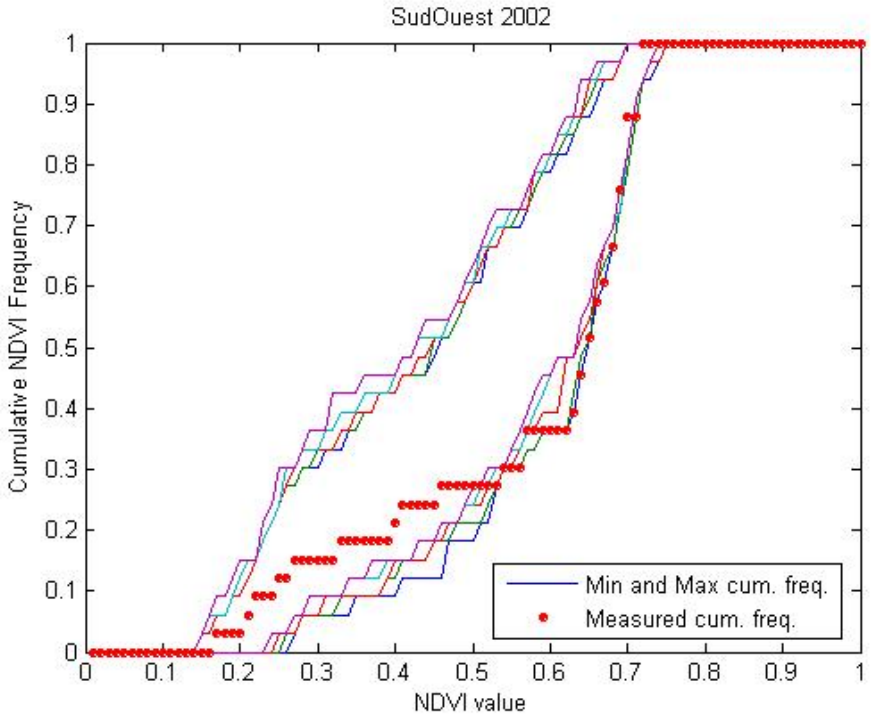

Figure 7. Comparison of the ESU NDVI distribution and the NDVI distribution over the whole image.

Figure 7 shows that the NDVI distribution of the 33 ESUs is quite good over the whole site (comprised between the 5 highest and lowest cumulative frequencies) even if the cumulative frequency curve is often close to the boundaries for high NDVI values. It reaches even the boundaries on several occasions. NDVIs lower than 0.17 have not been sampled although they are present in the image. Moreover, the site is quite homogeneous in terms of NDVI since the highest and lowest distributions are close.

2.3.3. Evaluation based on classification

A non supervised classification based on the k_means method (Matlab statistics toolbox) was applied to the reflectance of the SPOT image to distinguish if different behaviours on the image for the biophysical variable-reflectance relationship exist. A number of 5 classes was chosen (Figure 8).

Results show that the distribution of the classes on the image and on the ESUs is rather different. Classes 1, 2, 3 and 4 appear to be over-sampled whereas class 5 is very under-represented. Class 3 is mainly represented by three added ESUs (S1, S2 and S3) and class 4 by two added ESUs (S4 and S5). The five classes correspond to:

- class 1: soya bean, woodland (4 ESUs);
- class 2: poplars, fallow, grassland (5 ESUs);
- class 3: fully senesced or harvested wheat fields, fallow (4 ESUs);
- class 4: fully senesced or harvested wheat fields, fallow (3 ESUs);
- class 5: corn (irrigated or not), soya bean (irrigated or not), sunflowers (17 ESUs).

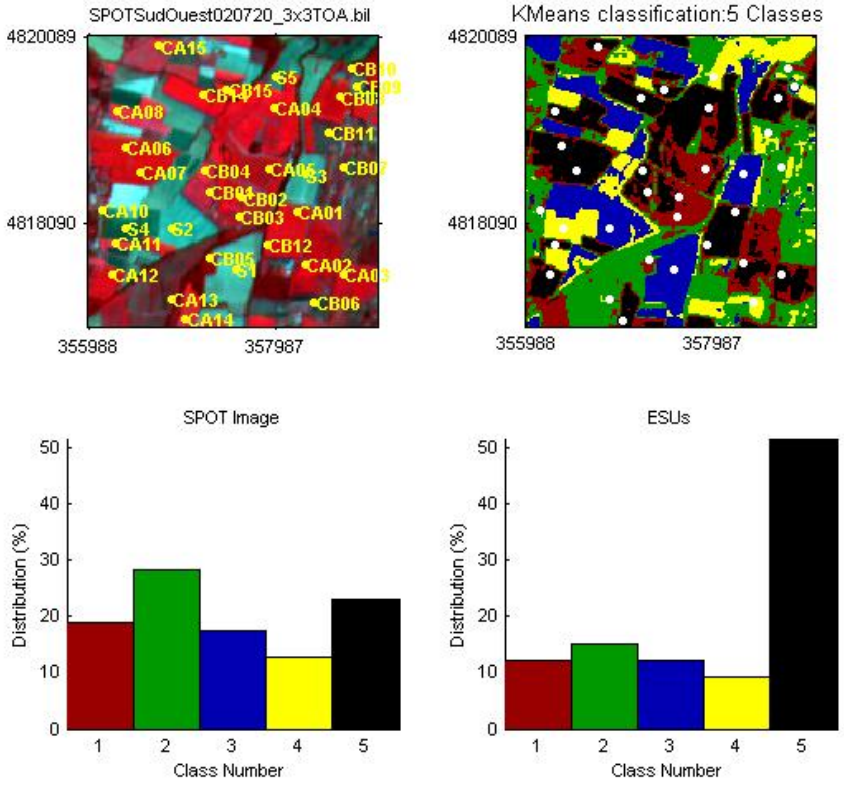

Figure 8. Classification of the SPOT image. Comparison of the class distribution between the SPOT image and sampled ESUs.

2.3.4. Using convex hulls

A test based on the convex hulls was also carried out to characterize the representativeness of ESUs. Whereas the evaluation based on NDVI values uses two bands (red and NIR), this test uses the four bands of the SPOT image. A flag image, is computing over the reflectances (Figure 8). The result on convex-hulls can be interpreted as:

- pixels inside the 'strict convex-hull': a convex-hull is computed using all the SPOT reflectance corresponding to the ESUs belonging to the class. These pixels are well represented by the ground sampling and therefore, when applying a transfer function the degree of confidence in the results will be quite high, since the transfer function will be used as an interpolator;
- pixels inside the 'large convex-hull': a convex-hull is computed using all the reflectance combination (±5% in relative value) corresponding to the ESUs. For these pixels, the degree of confidence in the obtained results will be quite good, since the transfer function is used as an extrapolator (but not far from interpolator);
- pixels outside the two convex-hulls: this means that for these pixels, the transfer function will behave as an extrapolator which makes the results less reliable. However, having a priori information on the site may help to evaluate the extrapolation capacities of the transfer function.

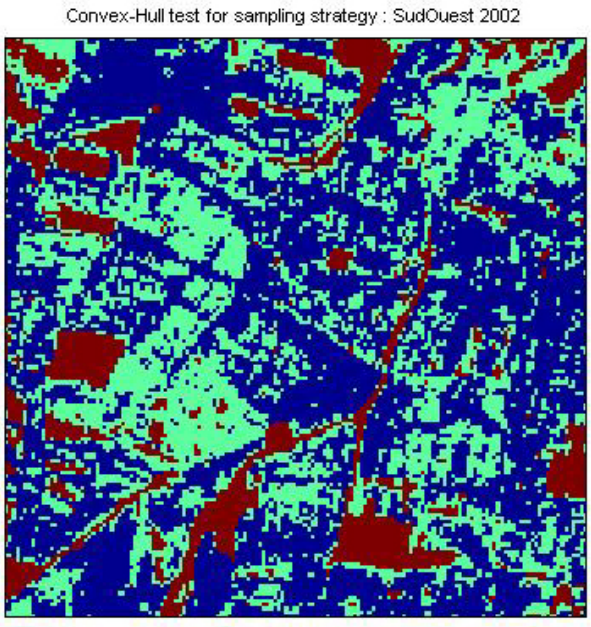

Figure 9. Evaluation of the sampling based on the convex hulls. Flag is shown at the bottom: blue and light blue correspond to the pixels belonging to the 'strict' and 'large' convex hulls and red to the pixels for which the transfer function is extrapolating.

The flag map shows that the representativeness of the ESUs is quite good, even if pixels are outside the two convex-hulls. They mainly correspond to bare soil, harvested wheat fields and woodland. The sampling is deficient on these types of cover.

3. Determination of the transfer function for the 6 biophysical variables: LAIeff, LAI57eff, LAItrue, LAI57true, fCover, fAPAR

3.1. The Transfer functions considered

For each class determined in §2.3, two types of transfer functions were tested:

- REG: If the number of ESUs is sufficient, multiple robust regression between ESUs reflectance (or Simple Ratio) and the considered biophysical variable can be applied: we used the 'robustfit' function from the matlab statistics toolbox. It uses an iteratively re-weighted least squares algorithm, with the weights at each iteration computed by applying the bisquare function to the residuals from the previous iteration. This algorithm provides lower weight to ESUs that do not fit well. The results are less sensitive to outliers in the data as compared with ordinary least squares regression. At the end of the processing, three errors are computed: classical root mean square error (RMSE), weighted RMSE (using the weights attributed to each ESU) and cross-validation RMSE (leave-one-out method).

- LUT: If the number of ESUs is sufficient, Look-Up-Tables are also enviewed: a look-up table is built using ESUs reflectances and the corresponding measured biophysical variable. For a given pixel, a cost function is computed as the sum of the square difference between the pixel reflectances and the ESU reflectances over the 4 bands, divided by the standard deviation computed on ESU reflectances. The result of the cost function is sorted in ascending order, and the biophysical variable estimated for the given pixel is computed as the mean value of the first *n* ESUs providing the lowest value of the cost function. Different values of *n* are considered to get the lowest cost function. This method is reliable only if the ESU NDVI distribution is quite comparable with the whole site NDVI distribution, which was quite the case for this Sud-Ouest site.

The regression and Look-Up-Tables are tested using either the reflectance or the logarithm of the reflectance for any band combination as well as the simple ratio. As both methods have poor extrapolation capacities, a flag image, based on the convex hulls is computing over reflectances (2.3.4).

3.2. Results

3.2.1. Choice of the method

For the 5 classes, a unique transfer function was computed. Figure 10 and Figure 11 show the results obtained for all the possible band combinations using either the reflectance or the logarithm of the reflectance:

- The REG method provides better results in terms of cross-validation RMSE for all the variables and is therefore selected as the transfer function instead of the LUT;
- For LAIeff, LAItrue, LAI57eff, LAI57true, fCover and fAPAR, the results using the reflectance are the best. Depending on the biophysical variable, the choice of the method proves to be difficult because the results are close.

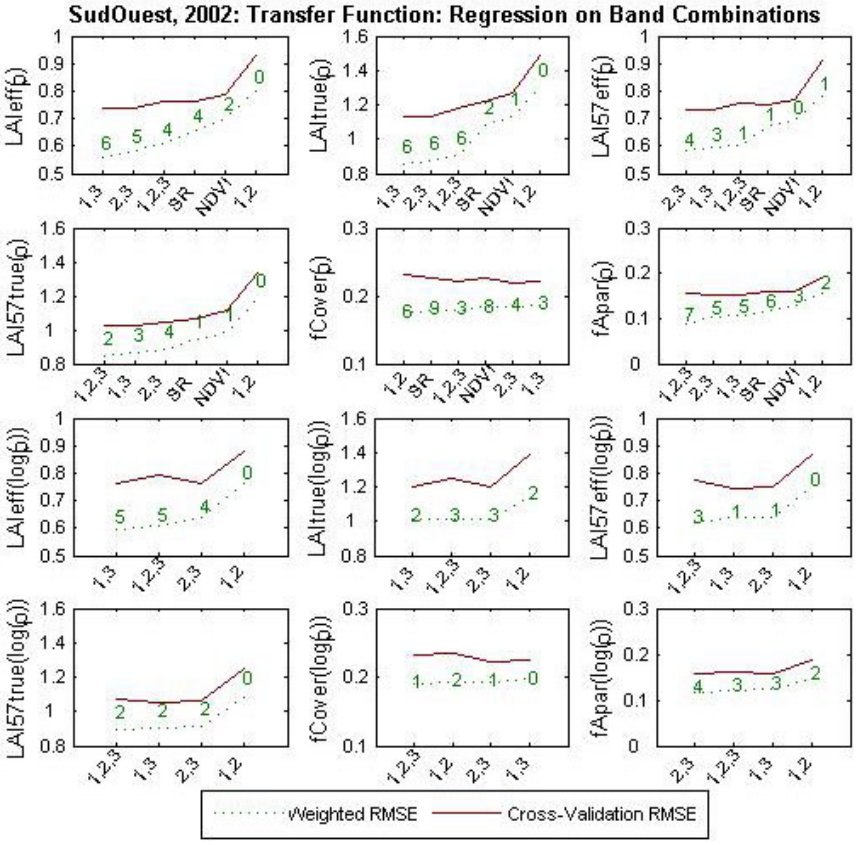

Figure 10. Transfer function: test of multiple regression applied on different band combinations. Band combinations are given in abscissa. The estimated biophysical variable is given in ordinate. Top graphs correspond to regression made on reflectance (ρ): the weighted root mean square error (RMSE) is presented in green along with the cross-validation RMSE in red. The numbers indicate the number of data used for the robust regression with a weight lower than 0.7 that could be considered as outliers. Bottom graphs correspond to regression made on the logarithm of the reflectance.

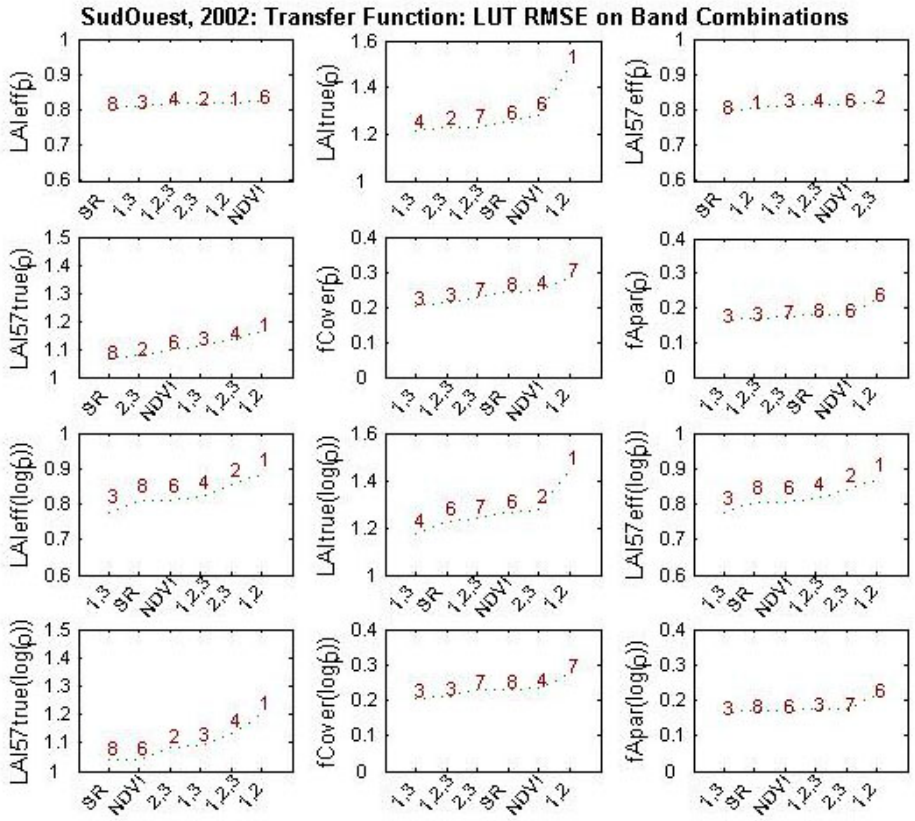

Figure 11. Transfer function: test of LUT applied on different band combinations. Band combinations are given in abscissa. The estimated biophysical variable is given in ordinate. Top graphs correspond to regression made on reflectance (ρ): the root mean square error is presented in green. The numbers indicate the number of elements selected in the LUT to compute the resulting biophysical variables. Bottom graphs correspond to LUT using the logarithm of the reflectance.

3.2.2. Choice of the band combination

For the LAIeff, the XS1, XS2, XS3 combination on reflectance was selected since it provides a good compromise.between the number of weights lower than 0.7 (four), the cross-validation RMSE value (among the lowest values) and the weighted root mean square error (Figure 12).

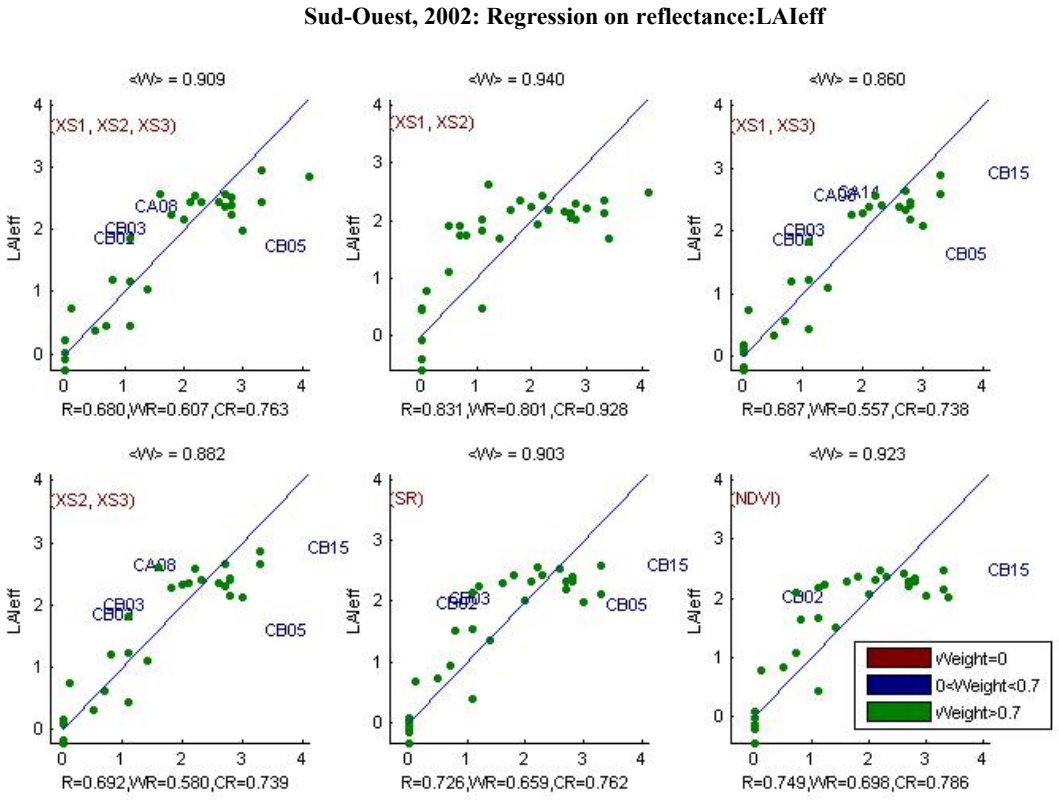

Figure 12. Effective Leaf Area Index: results for regression using different band combinations. R is the root mean square error computed between LAIeff and estimated LAIeff. WR is the weighted root mean square error and CR is the cross validation root mean square error.

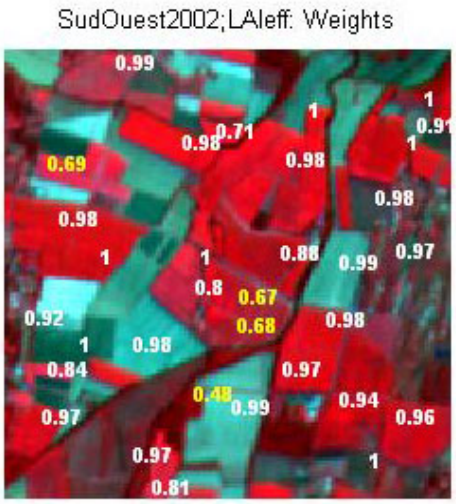

Figure 13. Weights associated to each ESU for the determination of LAIeff transfer function.

For the LAItrue, the XS1, XS3 combination on reflectance was selected since it provides the lowest cross-validation RMSE value and the lowest weighted root mean square error value. However, six ESUs have weights lower than 0.7 (Figure 14).

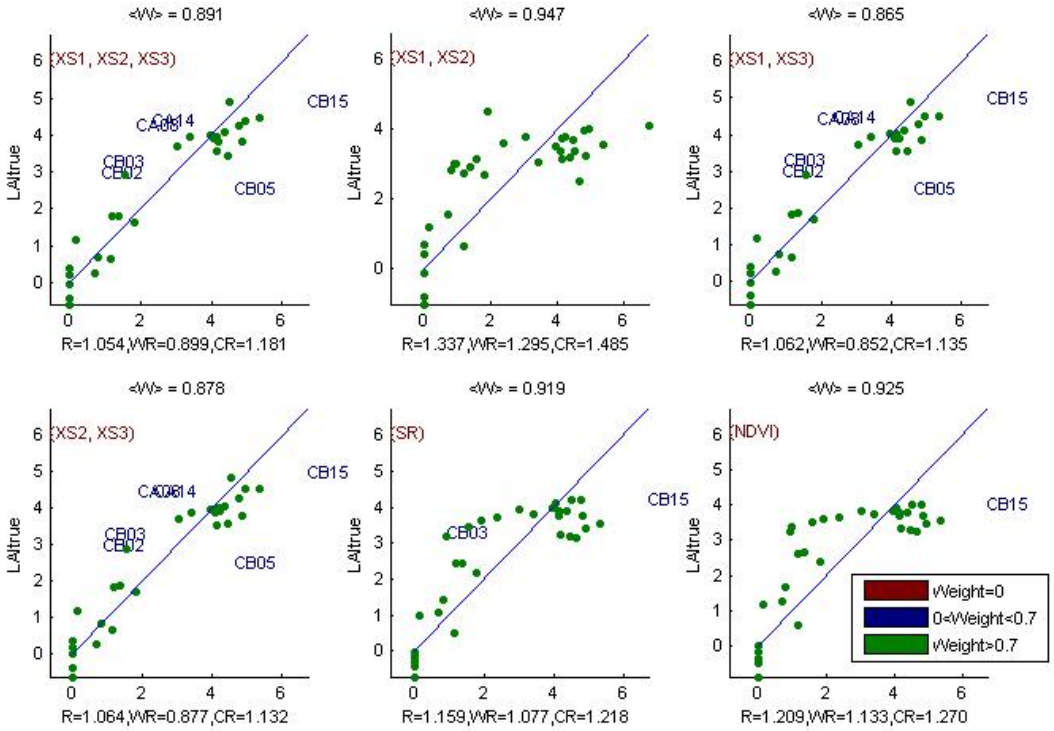

Figure 14. True Leaf Area Index: results for regression using different band combinations. R is the root mean square error computed between LAItrue and estimated LAItrue. WR is the weighted root mean square error and CR is the cross validation root mean square error.

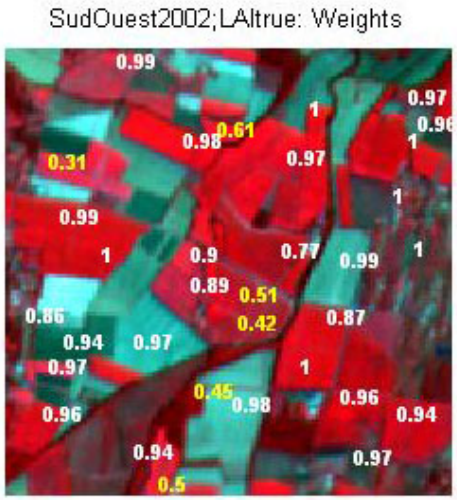

Figure 15. Weights associated to each ESU for the determination of LAItrue transfer function.

For the LAI57eff, the XS1, XS3 combination on reflectance was selected since it provides a good compromise (Figure 16) between the number of weights lower than 0.7 (three), the cross-validation RMSE value (the lowest value) and the weighted root mean square error (among the lowest values).

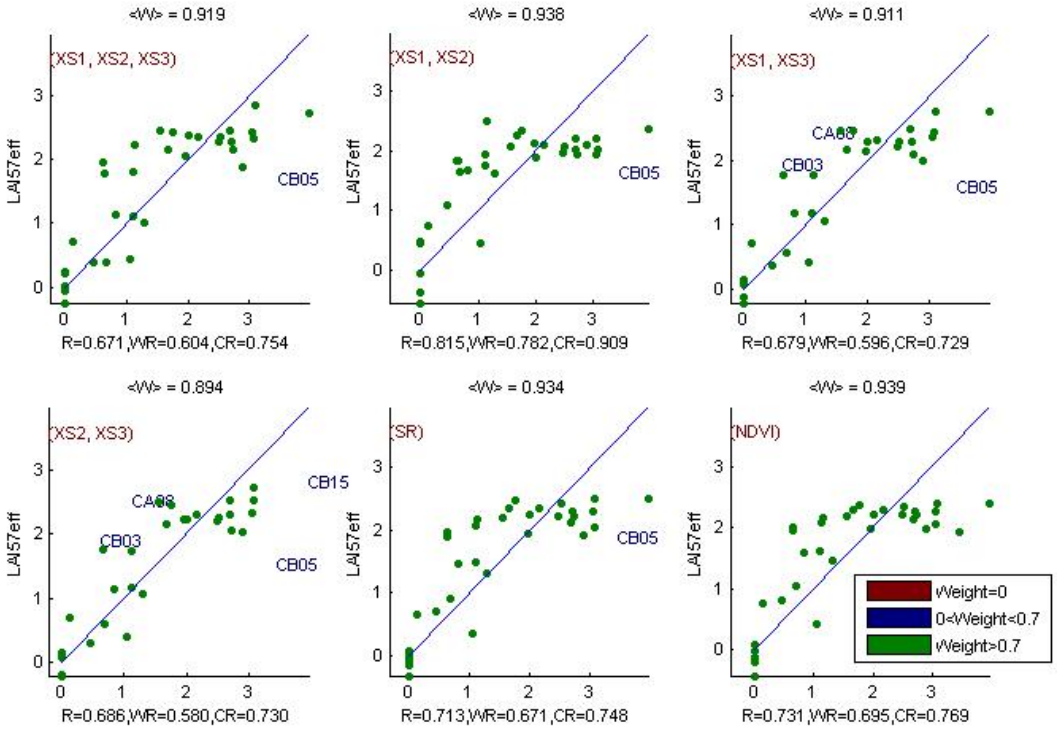

Figure 16. Effective Leaf Area Index at 57.5°: results for regression using different band combinations. R is the root mean square error computed between LAI57eff and estimated LAI57eff. WR is the weighted root mean square error and CR is the cross validation root mean square error.

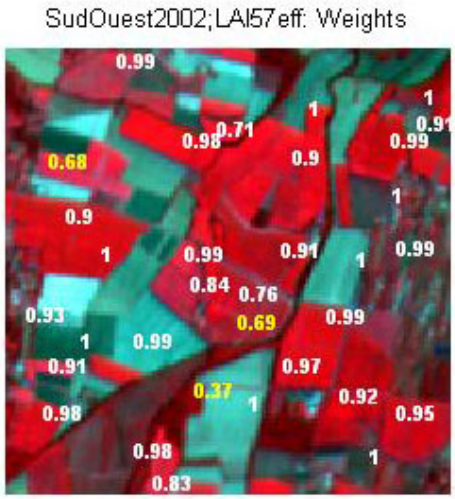

Figure 17. Weights associated to each ESU for the determination of LAI57eff transfer function.

For the LAI57true, the XS1, XS2, XS3 combination on reflectance was selected since it provides the best results: the lowest cross-validation RMSE value, the lowest weighted root mean square error value and two weights lower than 0.7 (Figure 18).

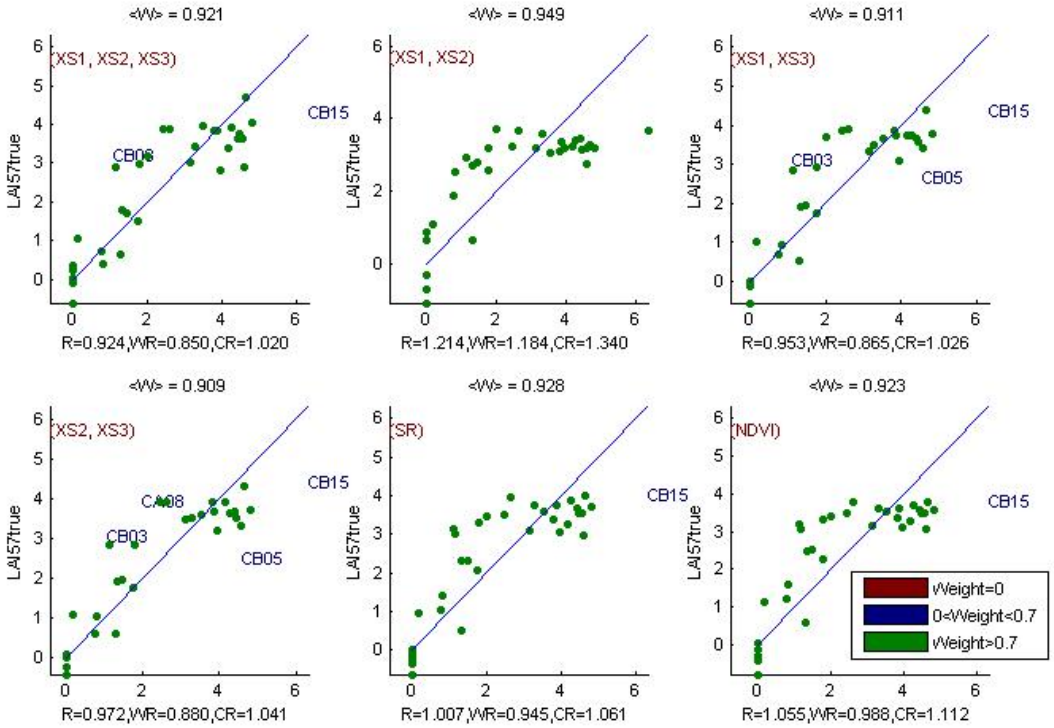

Figure 18. True Leaf Area Index at 57.5°: results for regression using different band combinations. R is the root mean square error computed between LAI57true and estimated LAI57true. WR is the weighted root mean square error and CR is the cross validation root mean square error.

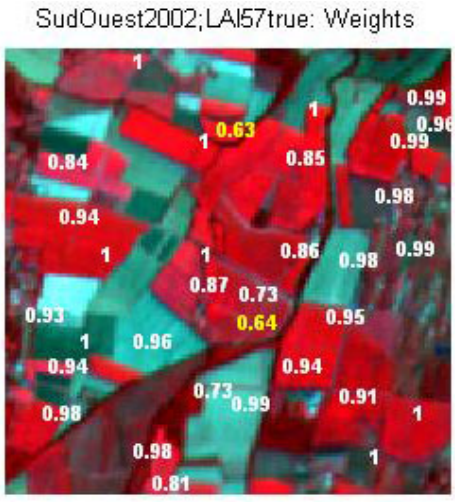

Figure 19. Weights associated to each ESU for the determination of LAI57true transfer function.

For the fCover, the XS1, XS2, XS3 combination on reflectance was selected since it provides a good compromise (Figure 20) between the number of weights lower than 0.7 (three), the cross-validation RMSE value (among the lowest values) and the weighted root mean square error (among the lowest values).

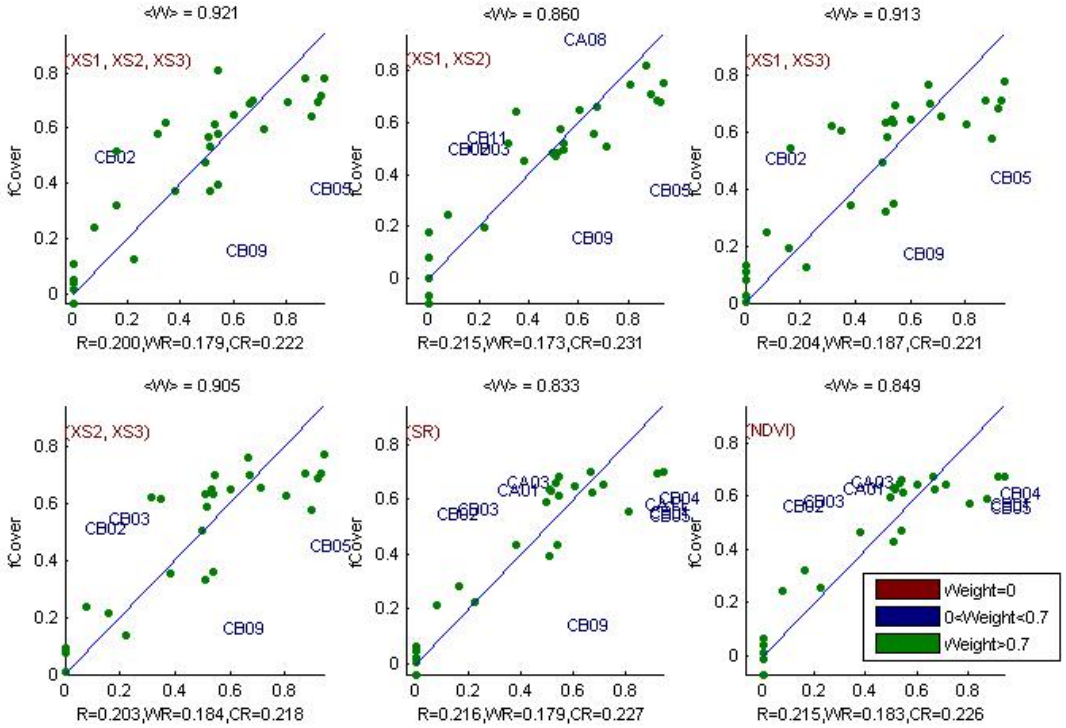

Figure 20. fCover: results for regression using different band combinations. R is the root mean square error computed between fCover and estimated fCover. WR is the weighted root mean square error and CR is the cross validation root mean square error.

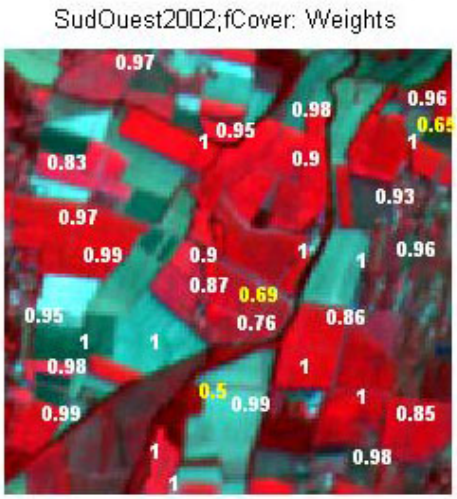

Figure 21. Weights associated to each ESU for the determination of fCover transfer function.

For the fAPAR, the XS2, XS3 combination on reflectance was selected since it provides a good compromise (Figure 22) between the number of weights lower than 0.7 (five), the cross-validation RMSE value (among the lowest values) and the weighted root mean square error (among the lowest values).

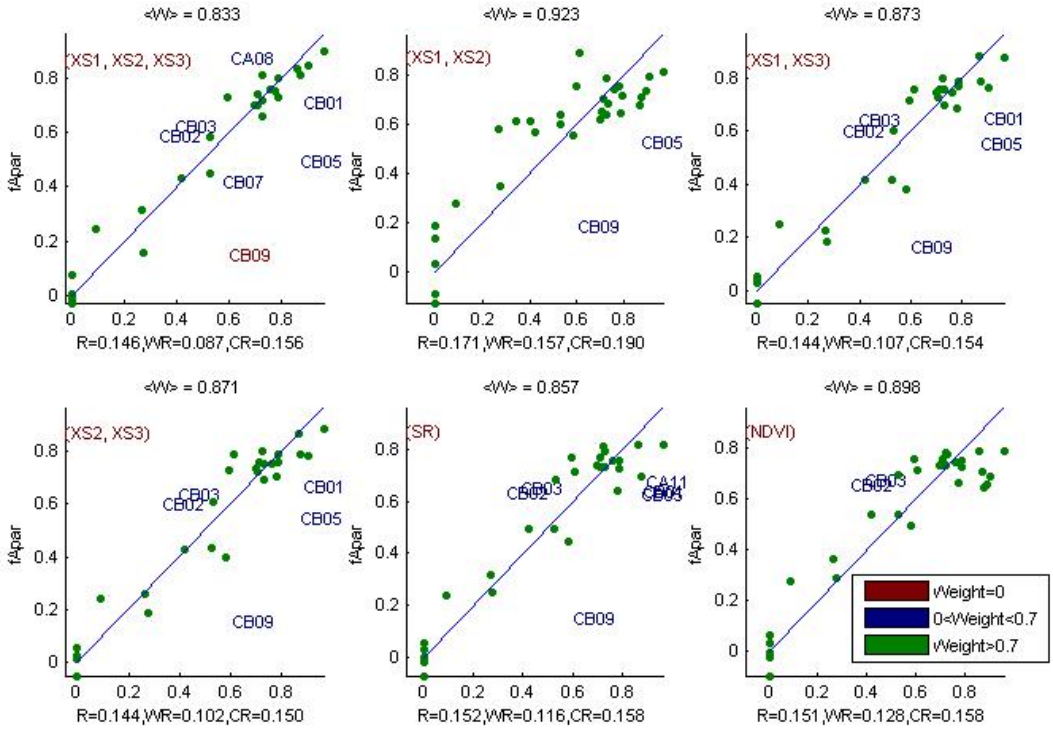

Figure 22. fAPAR: results for regression using different band combinations. R is the root mean square error computed between fAPAR and estimated fAPAR. WR is the weighted root mean square error and CR is the cross validation root mean square error.

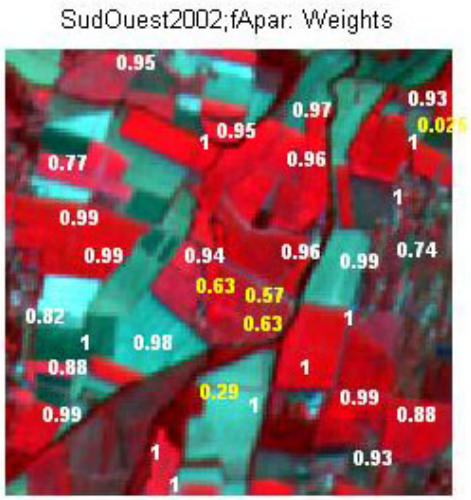

Figure 23. Weights associated to each ESU for the determination of fAPAR transfer function.

Following, the results of the transfer function (Table 2):

Variable	Band Combination	RMSE	Weighted RMSE	Cross-valid RMSE
LAIeff	0.40973 - 39.022(XS1) + 16.971(XS2) + 12.563(XS3)	0.680	0.607	0.763
LAItrue	-2.9994 - 11.73(XS1) + 21.546(XS3)	1.062	0.852	1.135
LAI57eff	-0.56126 - 12.68(XS1) + 10.897(XS3)	0.679	0.596	0.729
LAI57true	3.8133 - 120.5(XS1) + 60.764(XS2) + 20.779(XS3)	0.924	0.850	1.020
fCover	-1.1125 + 20.101(XS1) - 14.68(XS2) + 1.9058(XS3)	0.200	0.179	0.222
fAPAR	-0.080761 - 3.7306(XS2) + 2.86(XS3)	0.144	0.102	0.150

Table 2. Transfer function applied to the whole site for the different biophysical variables, and corresponding errors

3.3. Applying the transfer function to the Sud-Ouest SPOT image extraction

Figure 24 presents the biophysical variable maps obtained with the transfer function described in Table 2. The maps obtained for the six variables are consistent, showing similar patterns: low LAIeff values where low fCover or fAPAR are observed and conversely… The difference between effective LAI and true LAI is significant (see the average values in Figure 24). This was expected when looking the LAIeff/LAItrue relationship in Figure 24, showing that for high LAI the difference between the two can be significant.

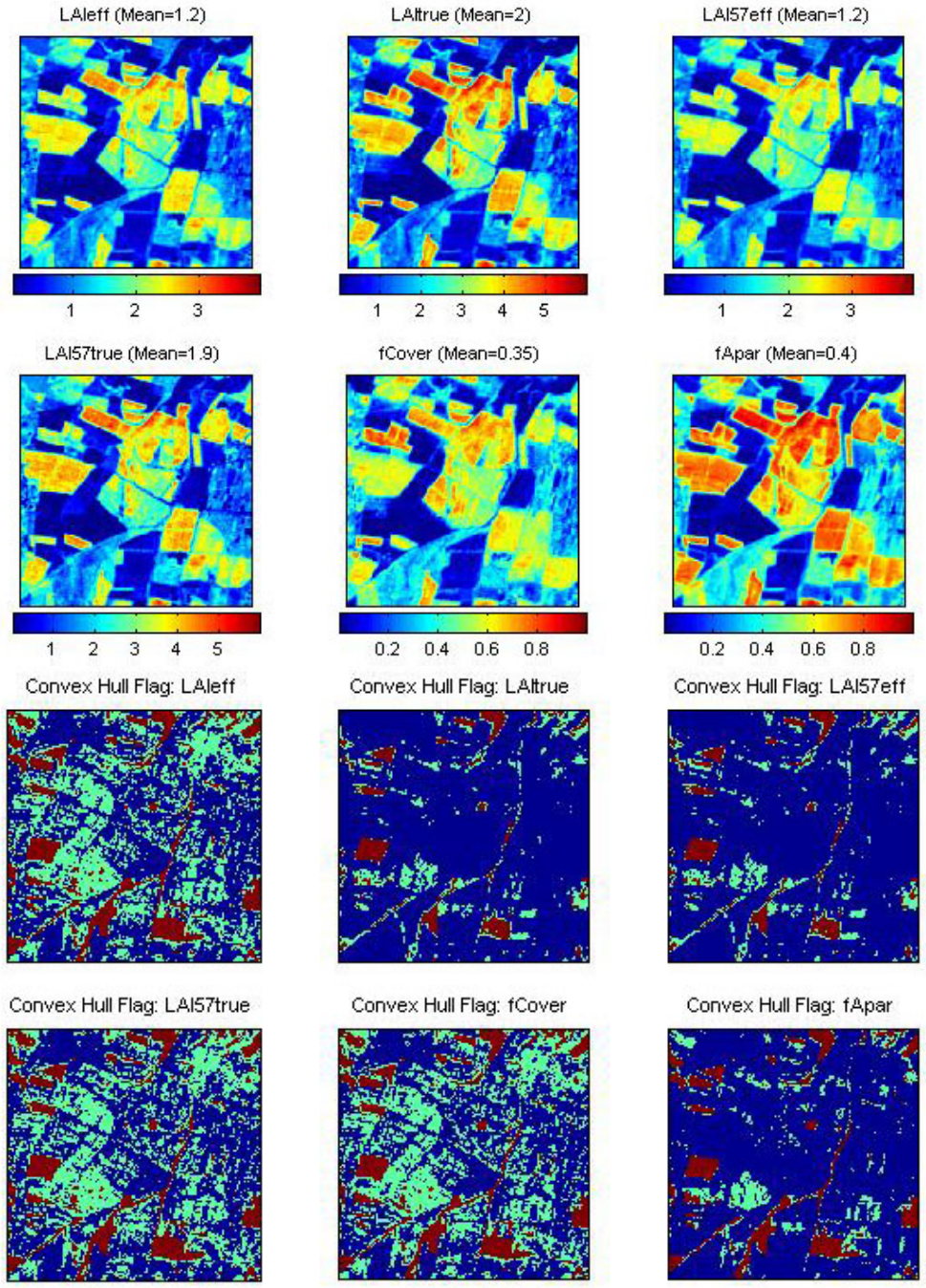

Figure 24. High resolution biophysical variable maps applied on the Sud-Ouest site (top). Associated Flags are shown at the bottom: blue and light blue corresponds to the pixels belonging to the 'strict' and 'large' convex hulls and red to the pixels for which the transfer function is extrapolating.

The flag maps are not very different between the biophysical variables. The results are comparable between LAIeff, LAI57true and fCover, but also between LAItrue, LAI57eff and fAPAR. The extrapolation of the transfer function is little all over the site. For LAItrue, LAI57eff and fApar, note that few pixels are outside the strict convex hull.

4. Conclusion

The transfer functions are obtained by using 33 ESUs. As the representativeness of the land cover by the different ESUs was not optimal, five ESUs (S1, S2, S3, S4 and S5) were added. They are located in wheat fields. The maps obtained for the biophysical variables are consistent and the flag associated to each map show that the transfer function is marginally used as an extrapolator. For all the variables, the regression coefficients are computed by relating the variable itself to the reflectance.

The biophysical variable maps are available in UTM, 31 North, projection coordinates (Datum: WGS-84) at 20m resolution.

5. Acknowledgements

We thank people who participated to the field experiment: **Gérard Dedieu**, **Philippe Maisongrande**, **Guillaume Maubert**, **Etienne Voisin** (CESBIO, Toulouse, France), **Ignacio Touriño Soto** (ESAT, Toulouse, France) and **Sébastien Garrigues** (INRA CSE, Avignon, France)

ANNEX

Ground measurement acquisition report for the VALERI site **Sud-Ouest**

sampled from 07/07/2002 to 08/07/2002

Sébastien Garrigues and Gérard Dedieu
Organization: INRA (Avignon), CESBIO (Toulouse)
email: gerard.dedieu@cesbio.cnes.fr,
sebastien.garrigues@avignon.inra.fr

Date of report 02/10/2002

People participating to the field experiment:

Fistname & Name	0rganization
Gérard Dedieu	CESBIO, Toulouse, France
Sébastien Garrigues	INRA CSE, Avignon, France
Phillippe Maisongrande	CESBIO, Toulouse, France
Guillaume Maubert	CESBIO, Toulouse, France
Ignacio Tourino Soto	ESAT, Toulouse, France
Etienne Voisin	CESBIO, Toulouse, France

Site coordinates

	Lat-Long WGS84 (Deg min.00)		UTM / WGS84 UTM 31 North		Other projection*	
	Lat.	Long.	Easting	Northing	East	North
Upper left corner	43.31	1.13	356002.44	4820075.31	509460	1835940
Lower right corner	43.29	1.152	359042.44	4817035.31	512460	1832940

*The other projection user is *Lambert II etendu.* All the characteristics are provided in the following table (see http://www.avignon.inra.fr/valeri/, methodology page, GPS document for more information):

Geodesic Map Datum : NTF		Map Projection: Lambert II etendu	
Associated Ellipsoïd	Clarke 1980 IGN	Application zone	France
Semi-major axe	6378249.2	Latitude of origin	44°48'N
Semi-minor axe	6356515.0	Longitude of origin	2°20'14.025" (Paris)
1/flattening	293.466021	Parallels: 1st 2nd	45°53'56.108" 47°41'45.652"
Eccentricity	0.08248325676		
		Xo: false easting	600 000 m
		Yo: false northing	2 200 000 m
		Scale factor	1

Ground control points

The Excel file GPSSudOuest2002.xls contains different waypoints (UTM/WGS84) acquired on the site:

GCP1	358240	4817743	La Mothe, road intersection
GCP2	356129	4819092	d12 and d82 road intersection
GCP4	358397	4818317	d12 and d50 road intersection
GCP5	356796	4819723	GCP, road and bridge intersection
GCP9	358039	4817705	La Mothe farm

GPS system used: Garmin etrex (team B) and MLR modèle SP 24 XC (team A)
Typical uncertainty of GPS position: 7 m.

Description of the site and land cover

Site Size

The site size is 3040m*3040m (152 SPOT pixels*152 SPOT pixels).

Category according to IGBP classification

Croplands.

Comments on the land cover

The land cover is composed mainly of: crops (corn, soyabean, sunflower) and grasslands. The fields have quite important size. The mean field size is about 15-20 ha.

Topography

The site is at about 170 m altitude. It is generally quite flat.

Land cover map

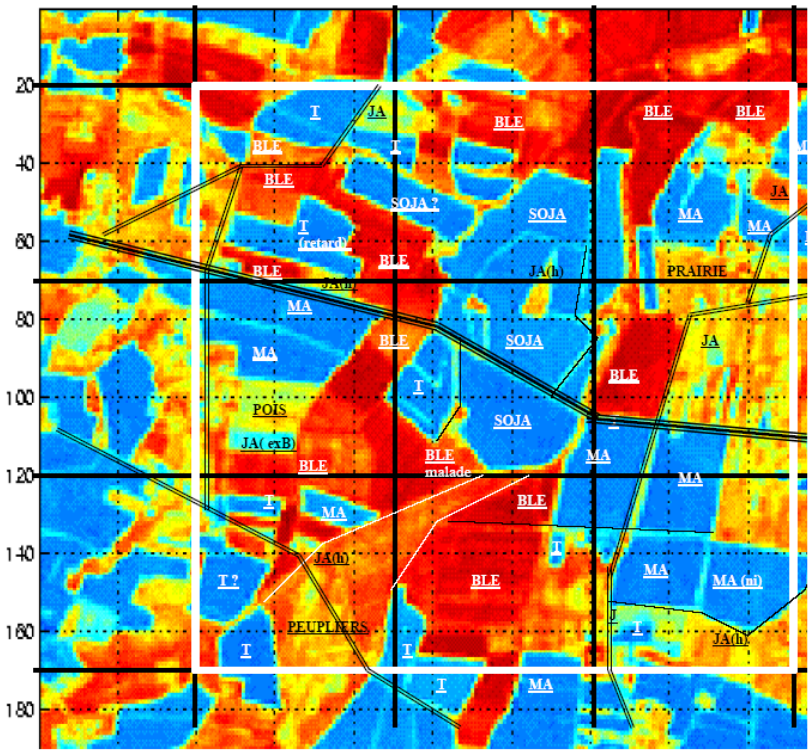

Legend

BLE	wheat
SOJA	soya
Peupliers	poplars
T	sunflower
Retard	late
JA	fallow
MA	maize
Prairie	grassland
Pois	pea

Spatial sampling scheme

Sensors used for sampling the ESUs

	Method	Comments
☒	Hemispherical photographs	
☐	LAI2000	
☐	TRAC	
☐	Ceptometer	
☐	Direct measurements	
☐	Other	

Sampling strategy for the ESU

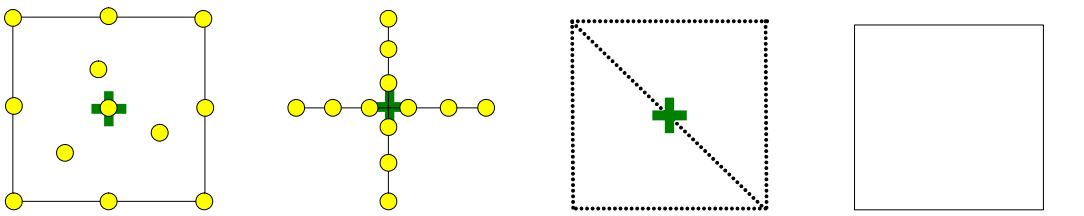

a ☐ **b** ☒ **c** ☐ **d** ☐ (specify)

Distribution of the Elementary sampling units

The crosses distribution was used.

The high spatial resolution image

Satellite

Satellite used SPOT2 HRV1
Level of processing 2B, SPOTView basic
Projection type UTM, zone 31, WGS84
Georeferencing comment (accuracy, waypoint validation …):
Comments: different images are available (please contact the person in charge with site):

- A 5*5 km SPOT image (*SPOTSudOuest020720_5x5km.bil*) centered on the site (UTM, 31 North, WGS84)
- A 3*3km SPOT image (*SPOTSudOuest020720_3x3km.bil*) (UTM, zone 31 North, WGS84)

Acquisition date: 20/07/2002 - 11:18:22

List of the ESUs

A GPS file (Excel file GPSSudOuest2002.xls) presents the list of the ESUS with different informations:

- ESU number (AXX or BXX, A and B are the team name)
- Month
- Day
- Hour
- Minute
- Pixel-id: the pixel (1km*1km of the 3km*3km site) number where the ESU falls.
- Easting
- Northing
- Latitude (same reference system than cartographic coordinate)
- Longitude
- Altitude
- GPS accuracy indicator (Hdop (m) or satellite number)
- 1st photo number: file number XXXX (of DSCNXXXX.JPG) of the ESU 1st hemispherical photo
- last photo number: file number (XXXX of DSCNXXXX.JPG) of the ESU last hemispherical photo
- total number of hemispherical photos
- crop type
- comments

easting(utm)	northing(utm)	crop_type	Comments on the vegetation status, condition of acquisitions, etc...
358240	4817743		La Mothe, road intersection
356129	4819092		d12 and d82 road intersection
358397	4818317		d12 and d50 road intersection
356796	4819723		GCP, road and bridge intersection
349026,71	4797106,73		road intersection, validity ??
348744,9	4796514,1		road intersection, validity ??
348426,96	4796846,79		road intersection, validity ??
358039	4817705		La Mothe house
356002,44	4820075,31		
359042,44	4817035,31		
358224	4818212	irrigated corn	
358305	4817664	irrigated corn	
358709	4817548	corn	small
357978	4819316	irrigated soya bean	irrigated on the day
357915	4818670	soya bean	row spacing =70cm, non irrigated
356397	4818903	irrigated corn	h=2.2<m, 12 leaves, row spacing=75cm
356556	4818644	irrigated corn	row spacing=75cm,h=2.10m
356315	4819286	sunflower	non irrigated , h=50cm,row spacing=80cm, irregular size
357291	4818432	sunflower	
357633	4818366	soya bean	
357605	4818165	soya bean	narrow field
357242	4818656	sunflower	small, young
357288	4817729	woodland	very developed understorey
358403	4817257	fallow	very heterogeneous, with different phenological states
358701	4818684	fallow	
356250	4819721	non irrigated corn	row spacing=75cm, h=40cm, weed on the floor
356150	4818232	cut grassland	presence of haystacks
356298	4817878	sunflower	1.80m, row spacing=70 cm
356265	4817555	irrigated corn	
356892	4817285	peuplier	h=7m,row spacing=7m, ploughland, weed
357036	4817077	young soyabean	non irrigated
356758	4819976	soya bean	not in flower
358668	4819433	corn	changing irradiance conditions for the photos
358842	4819547	fallow	heterogeneous, different phenological states (green, yellow)
357897	4817866	corn	irrigated, h=1.80 m, homogeneous, row spacing=70cm
358796	4819737	grassland	close to the woodland, short cut grass
358559	4819053	grassland	neighbouring houses, very short grass, different phenological states
358706	4819620	corn	narrow field
357219	4819461	corn	homogeneous, height=1.9m, some clouds
357474	4819513	sunflower	late development, heterogeneous, very variable height

Acknowledgements

Thanks to all the persons who participated to the field experiment. Thanks to the Ferme de Purpan LaMothe (Daniel Bataille), Sud-Ouest farmers (Mr Eric Jean-Pierre …) for their friendly welcome.

Photo gallery

#	File name	Comments
1	Teama.jpg	Team action
2	Afterlunch.jpg	Team after lunch
3	Cesbioteam.jpg	Team Picture
4	Tracteur.JPG	Team Picture
5	Siesta.JPG	Siesta after lunch
6	restau.JPG	SudOuest Restaurant

Additional comments

A very pleasant campaign !!